INTERNATIONAL JOURNAL FOR NUMERICAL METHODS IN FLUIDS
Int. J. Numer. Meth. Fluids 2003; **41**:133–150 (DOI: 10.1002/fld.430)

A new second-moment closure approach for turbulent swirling confined flows

Pisi Lu and Viriato Semião*,†

Instituto Superior Técnico, Mechanical Engineering Department, Av. Rovisco Pais, 1049-001 Lisbon, Portugal

SUMMARY

An improved anisotropic model for the dissipation rate—ε—of the turbulent kinetic energy (k), to be used together with a non-linear pressure-strain correlations model, is proposed. Experimental data from the open literature for two confined turbulent swirling flows are used to assess the performance of the proposed model in comparison to the standard ε transport equation and to a linear approach to model the pressure-strain term that appears in the exact equations for the Reynolds-stress tensor. For the less strongly swirling flow the predictions show much more sensitivity to the ε transport equation than to the pressure-strain model. In opposition, for the more strongly swirling flow, the results show that the predictions are much sensitive to the pressure-strain model. Nevertheless, the improved ε transport equation together with the non-linear pressure strain model yield predictions in good agreement with experiments in both studied cases. Copyright © 2003 John Wiley & Sons, Ltd.

KEY WORDS: Reynolds stress transport model; turbulence; anisotropic dissipation; pressure strain model; computational fluid dynamics; swirling flows

1. INTRODUCTION

Confined swirling flows are present in a vast range of industrial engineering applications, such as combustion chambers, in which turbulent swirl is likely to exert a significant influence on combustion performance, efficiency and pollutants formation. The ability to predict the characteristics and the properties of confined swirling flows is, therefore, of major importance. Although Computational Fluid Dynamics (CFD) predictive usually include many physical and mathematical models to simulate all the phenomena involved inside combustion chambers (turbulence, combustion and radiation), the turbulence model deserves particular attention as it describes the flow structure that, in turn, strongly influences all the

* Correspondence to: V. Semião, Instituto Superior Técnico, Mechanical Engineering Department, Av. Rovisco Pais, 1049-001 Lisbon, Portugal.
† E-mail:viriato@navier.ist.utl.pt

Contract/grant sponsor: European Collaborative Research JOULE Programme; contract/grant number: JOE3-CT97-0070
Contract/grant sponsor: Fundacão para a Ciência e Tecnologia; contract/grant number: PRAXIS XX1/BD/16094/98.

Received September 2001
Revised 15 July 2002

other determinant parameters. Therefore, the capability of a CFD code to predict accurately swirling, turbulent and reacting flows partly lies on the potential of its turbulence model.

The k–ε model [1] has been widely used in the computation of combusting turbulent flows [2–4]. Although this model has proved to perform well for simple flow cases, it is well known that its behaviour for complex swirling flows is rather poor. This flaw may emerge from the use of the isotropic eddy viscosity concept in the definition of the Reynolds stresses. In reality, swirling flows are usually highly anisotropic. The Reynolds stress transport model (hereafter RSTM), in turn, provides a direct route to evaluate the turbulent stresses through the solution of their respective transport equations, rather than using the isotropic eddy viscosity approach, which makes of it a more robust model. This model did not, however, cover all the deficiencies of the k–ε model in the prediction of swirling flows [5–7]. Indeed, it is presently well established that both the equation for the dissipation rate of k and the pressure-strain term lack of modelling improvements and are a source of inaccuracy in predicting turbulent quantities [8–10].

Both k–ε model and standard RSTM make recourse to a transport equation for the turbulent kinetic energy dissipation rate, ε, as primarily presented for high Reynolds numbers flows. It has been argued in the open literature that mean shear terms have no proper place in an ε transport equation, since the dissipation process concerns to fine-grained turbulence. In fact, and according to Reference [8], as the mean shear deforms the large-scale eddies, so must anisotropies in the large-scale eddies be expected to stretch eddies to somewhat finer scales and thus contribute to the rate of the energy cascade across the spectrum. Therefore, some of the stress anisotropy invariants ought to appear in the ε transport equation. In their work [11], the authors proposed to model the source term of the ε transport equation solely in terms of the turbulence anisotropy second invariant. Although well argued, the idea did not prove to be very helpful when applied to real flows.

Turbulence comprises fluctuating motions with a spectrum of sizes and time scales. Different turbulent interactions are known to be associated with the different parts of the energy spectrum. At high Reynolds numbers the energy in turbulent flows is produced by mean strain at low wave numbers and it is dissipated at considerably higher wave numbers characteristic of the dissipative eddies. The rate of energy transfer from productive large-eddies to dissipative small-eddies depends on the production itself and is, therefore, subjected to the degree of the anisotropy of the flow. Based on this concept, where the process of turbulent kinetic energy transfer from large-scale to small-scale eddies is controlled by anisotropy in swirling flows, a new anisotropic dissipation rate model is proposed herein. With this new approach, a modified source term of the ε transport equation based on physical reasoning is obtained. This modification establishes that anisotropy is responsible for the turbulence transfer from large-scale to small-scale eddies in regions of predominant anisotropic turbulence. On the other hand, in flow regions where turbulence is predominantly isotropic, isotropy controls the turbulent kinetic energy transfer through the cascade and this is also taken into account in the new approach.

Another flaw of the standard RSTM is the modelling of the pressure strain term of the Reynolds stresses transport equations. An advanced modelling strategy for the pressure-strain term was proposed [12] (SSG hereafter), which is non-linear in the Reynolds stresses. Such model has already yielded accurate results in different types of flows: both for wall-bounded flows without the use of empirical wall-reflection terms [13] and for free turbulent jets with

and without swirl [14]. This model is also implemented in the present work together with the new dissipation rate transport equation mentioned above.

Two isothermal flows in axially symmetric model combustors, one exhibiting a single inlet and the other a double concentric inlet system, which were both experimentally investigated, [15] and [16] respectively, are simulated in the present work. The predicted results are compared against the corresponding experimental data. For comparison purposes against the presently proposed model, predictions are also performed making recourse to another two Reynolds stresses transport models: the standard RSTM [17], LRR hereafter, that was later improved [18], and the above-mentioned standard SSG model. The performance of the different models in predicting the referred confined swirling flows is analysed. The results show that the new proposed approach for the ε transport equation, together with the SSG pressure-strain modelling, yielded predicted results with a considerable enhancement in accuracy for relatively weakly swirling flows (swirl number of 0.5, the swirl number S being defined by $S = \int_0^R UWr^2\,\mathrm{d}r/R\int_0^R U^2 r\,\mathrm{d}r$). For strongly swirling flows (swirl number of 2.25) the improvement in accuracy of the results emerges mainly from the use of the SSG model and the new proposed approach for the ε transport equation showed to have a pale contribution to the accuracy enhancement.

2. THE MATHEMATICAL AND PHYSICAL MODELLING

With the Reynolds decomposition, the mean transport equation for momentum in a steady-state flow can be derived from the instantaneous Navier–Stokes equations and may be expressed in tensor notation as

$$\frac{\partial}{\partial x_j}(\rho U_i U_j) = -\frac{\partial p}{\partial x_i} + \frac{\partial}{\partial x_j}\left(\mu\frac{\partial U_i}{\partial x_i} - \rho\overline{u_i' u_j'}\right) \tag{1}$$

On the right hand side of the previous equation the correlations between velocity fluctuations, the Reynolds stresses, are unknown. Further differential equations for the turbulent correlations can be obtained. However, these equations contain other correlations of higher (third) order. Among the several possibilities to close the system of the time-averaged equation (1) the RSTM was chosen in the present work due to its higher potential to correctly simulate the anisotropy of turbulent swirling flows, as mentioned in the introduction.

RSTM solves transport equations for each component of the Reynolds stresses ($\overline{u_i' u_j'}$) and it has been recognized as the most comprehensive description of turbulent flows that can be employed for practical computations with the present generation of computers.

The exact equations governing the transport of Reynolds stresses in a turbulent incompressible fluid flow may be written as (see, e.g. Reference [17]):

$$\begin{aligned}\frac{\partial U_k \rho\overline{u_i' u_j'}}{\partial x_k} = &-\left(\rho\overline{u_i' u_k'}\frac{\partial U_j}{\partial x_k} + \rho\overline{u_j' u_k'}\frac{\partial U_i}{\partial x_k}\right) - 2\mu\overline{\frac{\partial u_i'}{\partial x_k}\frac{\partial u_j'}{\partial x_k}} + \overline{p'\left(\frac{\partial u_i'}{\partial x_j} + \frac{\partial u_j'}{\partial x_i}\right)} \\ &- \frac{\partial}{\partial x_k}\left(-\mu\frac{\partial\overline{u_i' u_j'}}{\partial x_k} + \rho\overline{u_i' u_j' u_k'} + \overline{p'(\delta_{jk}u_i' + \delta_{ik}u_j')}\right)\end{aligned} \tag{2}$$

where δ_{ij} is the Kronecker operator.

Table I. Constants for the standard Reynolds stress transport turbulence model (LRR).

C_1	C_2	C_1'	C_2'	C_s	C_ε	$C_{\varepsilon 1}$	$C_{\varepsilon 2}$
3.0	0.5	0.75	0.5	0.22	0.15	1.4	1.8

A compact form of the above equation can be written as: $C_{ij} = P_{ij} + \Phi_{ij} + D_{ij} - \varepsilon_{ij}$, $C_{ij}, P_{ij}, \Phi_{ij}$, D_{ij}, and ε_{ij} being, respectively, the convection, the production, the pressure-strain correlation, the diffusion and the dissipation terms.

Based on a suggestion from a previous work [18], the diffusion term D_{ij} is modelled herein assuming that the diffusion transport rate of the Reynolds stresses is proportional to their gradients, that is, $D_{ij} = (\partial/\partial x_k)\left(\left(\mu\delta_{mk} + \rho C_s \overline{u_k' u_m'} k/\varepsilon\right) \partial \overline{u_i' u_j'}/\partial x_m\right)$, where C_s is a model constant.

The dissipation term (ε_{ij}) is modelled by assuming the dissipative motion as isotropic (see, e.g. Reference [17]), yielding $\varepsilon_{ij} = \frac{2}{3}\rho\varepsilon\delta_{ij}$. This dissipative term corresponds to the largest wave numbers in the energy spectrum of turbulence where viscous effects of dissipation are dominant.

The modelling of the pressure-strain term runs (after Reference [9]):

$$\Phi_{ij} = \Phi_{ij,1} + \Phi_{ij,2} + \Phi_{ij,w} \tag{3}$$

This term, however, still remains a subject of most controversy and experimental work is still being performed presently in order to have insight on the physical process of such phenomenon. A comprehensive model is usually decomposed into three parts, as in the exact Poisson equation for the pressure fluctuations. According to other studies (e.g. Reference [9]), the first two terms, $\Phi_{ij,1}$ and $\Phi_{ij,2}$, are strictly the volume integrals of the two point correlations, whereas the third term, $\Phi_{ij,w}$, represents the surface integral and is effective only in the vicinity of a solid wall or at an interface surface. Various approaches for modelling each of those terms were put forward over the years. Since the ultimate objective of this study is to propose a model which will be applicable to confined swirling flows encountered in practical applications, attention is confined to the linear model LRR and to the quadratic model SSG.

The LRR model: This model is essentially composed by the sub-models described below.

The first term is the return to isotropy term and it is calculated from the following approach [19]: $\Phi_{ij,1} = -C_1\rho(\varepsilon/k)(\overline{u_i' u_j'} - \frac{2}{3}k\delta_{ij})$. The second term is the rapid term and it is calculated from [20]: $\Phi_{ij,2} = -C_2\rho(P_{ij} - \frac{1}{3}P\delta_{ij})$.

The last term refers to the wall boundary modification, which consists of separate corrections to be made to $\Phi_{ij,1}$ and $\Phi_{ij,2}$. These corrections are expressed by (see, e.g. References [21, 22]), $\Phi^1_{ij,w} = C_1'\rho(\varepsilon/k)(\overline{u_l' u_m'} n_l n_m - \frac{3}{2}\overline{u_l' u_j'} n_l n_i - \frac{3}{2}\overline{u_l' u_i'} n_l n_j) f$ and $\Phi^2_{ij,w} = C_2'(\Phi_{lm,2} n_l n_m \delta_{ij} - \frac{3}{2}\Phi_{il,2} n_l n_i - \frac{3}{2}\Phi_{jl,2} n_l n_j) f$, where f is the wall damping function. This function has two components, $f_x = C_\mu k^{3/2}/(\kappa\varepsilon x_n)$ and $f_y = C_\mu k^{3/2}/(\kappa\varepsilon y_n)$, C_μ being a constant and x_n and y_n the axial and radial distances to the wall, respectively.

The constants used for the LRR model in the present study are those used previously in a similar work [23] and are listed in Table I.

Table II. Constants for the Reynolds stress transport turbulence model (SSG).

C_1	C_2	C_1^*	C_3	C_3^*	C_4	C_5	C_s	C_ε	$C_{\varepsilon 1}$	$C_{\varepsilon 2}$
3.4	4.2	1.8	0.8	0.325	1.25	0.4	0.22	0.183	1.44	1.83

The SSG model: In the SSG model, the pressure-strain correlation term, Φ_{ij}, is modelled after the application of various kinematics constraints yielding [12]:

$$\Phi_{ij} = -(C_1\varepsilon + C_1^*\mathrm{P})b_{ij} + C_2\varepsilon(b_{ik}b_{kj} - \tfrac{1}{3}b_{kl}b_{kl}\delta_{ij}) + (C_3 - C_3^*A_2^{1/2})kS_{ij} + C_4k(b_{ik}S_{jk} + b_{jk}S_{ik} - \tfrac{2}{3}b_{kl}S_{kl}\delta_{ij}) + C_5k(b_{ik}W_{jk} + b_{jk}W_{ik}) \quad (4)$$

In Equation (4), $P = -\overline{u_i'u_j'}(\partial U_i/\partial x_j)$ is the turbulent kinetic energy production, $A_2 = 4b_{ij}b_{ij}$ is the second invariant of anisotropy, $b_{ij} = \overline{u_i'u_j'}/\overline{u_q'u_q'} - \delta_{ij}/3$ is the Reynolds stress anisotropic tensor, the mean rate of the strain tensor is $S_{ij} = 1/2(\partial U_i/\partial x_j + \partial U_j/\partial x_i)$ and $W_{ij} = 1/2(\partial U_i/\partial x_j - \partial U_j/\partial x_i)$ is the mean vorticity tensor.

The SSG model constants are listed in Table II ([14]).

The transport equation of ε: The turbulent kinetic energy dissipation rate, ε, appearing in the modelling of the diffusion, redistribution and dissipation of the Reynolds stresses, is determined from its own transport equation which takes the following tensor notation form:

$$\frac{\partial}{\partial x_k}(U_k\varepsilon) = C_\varepsilon\frac{\partial}{\partial x_k}\left(\frac{k}{\varepsilon}\overline{u_k'u_l'}\frac{\partial\varepsilon}{\partial x_i}\right) + \frac{\varepsilon}{k}(C_{\varepsilon 1}P - C_{\varepsilon 2}\varepsilon) \quad (5)$$

It is well known that the dissipation rate of the turbulent kinetic energy is not properly modelled, being the most probable source of inaccuracies in predicting turbulent quantities. In previous works (References [6, 7]) it was found that the turbulent intensity obtained from the RSTM was much smaller in regions of the flow field predominantly isotropic than that yielded by using the isotropic k–ε model. This RSTM feature yields exaggerated radial gradients of the chemical species and the temperature profiles for isotropic turbulent regions, when compared to the corresponding experimental data. The reason for that may come from the inadequate modelling of the turbulence energy dissipation rate. In fact, Equation (5) overestimates the value of the dissipation rate of the turbulent kinetic energy. As a consequence, there is an underestimation of the turbulence intensity and a lower level of the turbulent mixing rate is estimated in such regions where turbulence is predominantly isotropic.

Numerous corrections and alternatives to the form of this equation have been proposed over the years [24–26]. Unfortunately, none of these approaches appears to have been tested over a wide range of flows, and, in the cases that tests were performed, those approaches have yielded worse predictions than the standard model.

An improvement to the equation for the transport of the dissipation rate of the turbulent kinetic energy, ε, was later recommended [8]. This improvement consisted of the inclusion of the turbulence anisotropy second invariant through the replacement of $C_{\varepsilon 2}$ by the function $1.92/(1 + 0.7AA_2^{0.5})$, where $A = 1.0 - 9.0/8.0(A_2 - A_3)$ and $A_3 = 8.0\ b_{ij}\ b_{jk}\ b_{ki}$, and making $C_{\varepsilon 1}$ equal to unity instead of the standard value $C_{\varepsilon 1} = 1.44$. The term A in the previous equations can provide a measure of the anisotropy of the flow. This parameter will always assume

values between zero and unity, the anisotropy being more pronounced in the regions of lower values of the above-mentioned A parameter. Although the effect of the turbulent kinetic energy production, P, is diminished through the decrease of the constant value of $C_{\varepsilon 1}$ (from 1.44 to 1.0, as mentioned above) and the effect of anisotropy is now involved through the function that replaced $C_{\varepsilon 2}$, this approach is still based on the concept of the standard model. Moreover, such approach maintains the mean strain affecting the dissipation rate through the term P, similarly to what is used in the transport equation for the turbulent kinetic energy, k [1].

In the present study, and based on the physical reasoning concept that anisotropy in the large-scale eddies controls the rate of turbulence energy transfer from large to small dissipative eddies as explained before, a new set of coefficient functions is proposed. In this new approach the constant $C_{\varepsilon 1}$ is replaced by the coefficient function $C_{\varepsilon 1}A_2$ and $C_{\varepsilon 2}$ is kept constant. The constant $C_{\varepsilon 2}$ has taken values between 1.8 and 1.92 based on calculations over data on decaying isotropic turbulent flows. Herein, the value of $C_{\varepsilon 2}$ was kept at 1.92. Based on experimental data [27], the value of $C_{\varepsilon 1}A_2$ was determined to be between 1.506 and 1.534. Moreover, $C_{\varepsilon 1}$ can be determined from $C_{\varepsilon 1}=(1+(C_{\varepsilon 2}-1)/(P/\varepsilon))/A_2$, which leads to a value of $C_{\varepsilon 1}$ between 3.63 and 3.80. Nevertheless, more accurate results were obtained in the present study by tuning the value of $C_{\varepsilon 1}$ to 2.88.

The term A_2P replaces that of P in Equation (5) and becomes dominant in regions of anisotropic turbulence. In such regions, the anisotropy feature of the turbulent flow strongly accelerates the transfer process rate of the turbulent kinetic energy from the mean flow large eddies to the small dissipative eddies, when compared to the transfer rate of isotropic turbulence. It is therefore expected that this turbulence feature will be more accurately predicted with such approach, A_2P, for the source term of the ε transport equation. On the other hand, in flow regions where turbulence is predominantly isotropic, i.e. regions of slower energy transfer rate, the function A_2 of the term A_2P in Equation (5) becomes insignificant. Therefore, the term $C_{\varepsilon 2}\varepsilon$ in that equation, which acts as a sink of the dissipation rate of ε, becomes dominant and, consequently, the transfer process of the turbulent kinetic energy gets slower. Hence, in regions of isotropic turbulence, the present approach is also expected to yield results as accurate as those yielded by the isotropy-based k–ε turbulence model.

Wall boundary conditions: The above second-moment closures are only applicable to high-Reynolds number flows and require the use of a sub-model covering the near-wall region.

In regions sufficiently close to the wall, generation of k and its dissipation rate are assumed to balance, this balance yielding the ε wall boundary condition [1].

The standard log-law for boundary layers [1] is used for the grid nodes next to the solid walls for the velocity components parallel to the walls, for the turbulent kinetic energy and for both the normal and shear stresses.

Typical values of the log-law local Reynolds number—dimensionless distance of the nearest grid node to the wall—ranged between 16 and 30 for case 1 (grid 96×68), and between 19 and 40 for case 2 (grid 48×52).

3. RESULTS AND DISCUSSION

In the present work two different geometries with isothermal, turbulent and swirling flows are numerically simulated.

Case 1: The first geometry studied herein—case 1—is sketched in Figure 1 and corresponds to the dump combustor for which flow experimental data exist [15]. The considered domain is

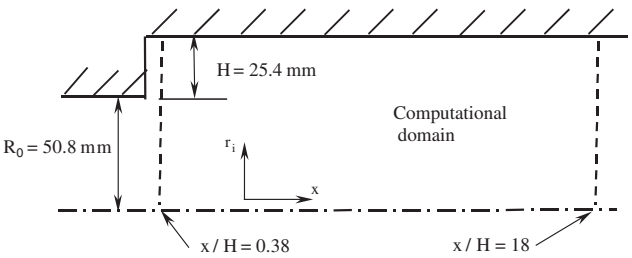

Figure 1. Sketch of the studied dump combustor geometry: case 1 (Reference [15]).

a portion of a cylindrical combustor chamber. The inlet pipe has a radius of $R_0 = 50.8$ mm and the combustor chamber has an inner radius of $R_i = 76.2$ mm and a total length of 1850 mm. The inlet centreline velocity has a value of $U_{\text{ref}} = 19.2$ m/s. Three different swirlers of the type of constant angle and axial flow yield flows with swirl numbers of $S = 0.0$, 0.3 and 0.5. The case corresponding to $S = 0.5$ was chosen to be simulated in present study as it is the most anisotropic flow and, therefore, the most appropriate for RSTM validation purposes.

Grid independence tests were performed by using two sets of grids comprising 48×34 nodes and 96×68 nodes, respectively, in the axial and radial directions. The results showed no noticeable differences. Therefore, only the predictions with the 96×68 grid are displayed. The non-uniform grid was made particularly denser near the inlet and close to both the burner lip and the wall.

As the purpose of the present study is to assess the accuracy of the Reynolds stress turbulence model, the domain was limited to the region between the axial stations $x/H = 0.38$ and 18, where $H = R_i - R_0$, as indicated in Figure 1. Those stations are the first upstream and the last downstream positions at which measurements for U, V, W, $\overline{u'^2}$, $\overline{v'^2}$, $\overline{w'^2}$, $\overline{uv}$ and $\overline{uw}$ are available. The experimental profiles of those quantities are used to specify the inlet and outlet boundary conditions. Additionally, $\overline{v'w'}$ is assumed to be zero at both the inlet and the outlet. The decision to use the available experimental data as inlet and outlet boundary conditions was taken in order to minimize the sources of possible errors in the predictions, similarly to what has been done by other authors that have predicted this type of flows (e.g. References [28–31]).

Three models were chosen for the simulation of this case study, in order to evaluate and compare the performance of different pressure-strain and turbulent kinetic energy dissipation rate approaches. The chosen models are: the standard RSTM (LRR) with the constants of Reference [23] (model 1 hereafter), the standard SSG model (model 2 hereafter) and the standard SSG model together with the new proposed transport equation of ε, Equation (5) with the modified source term, hereafter designated as model 3.

Computational results are compared against experimental data, in Figures 2–4. Generally, an overall agreement between the predictions and the experimental data for mean velocities, normal stresses and shear stresses is observed. However, model 3 allowed for improvements in the results accuracy, as explained below.

Measured and predicted non-dimensional radial profiles of the mean velocity components are compared in Figure 2. The experiments evidence the trend of the flow to flatten rapidly along the main flow direction for all the velocity components.

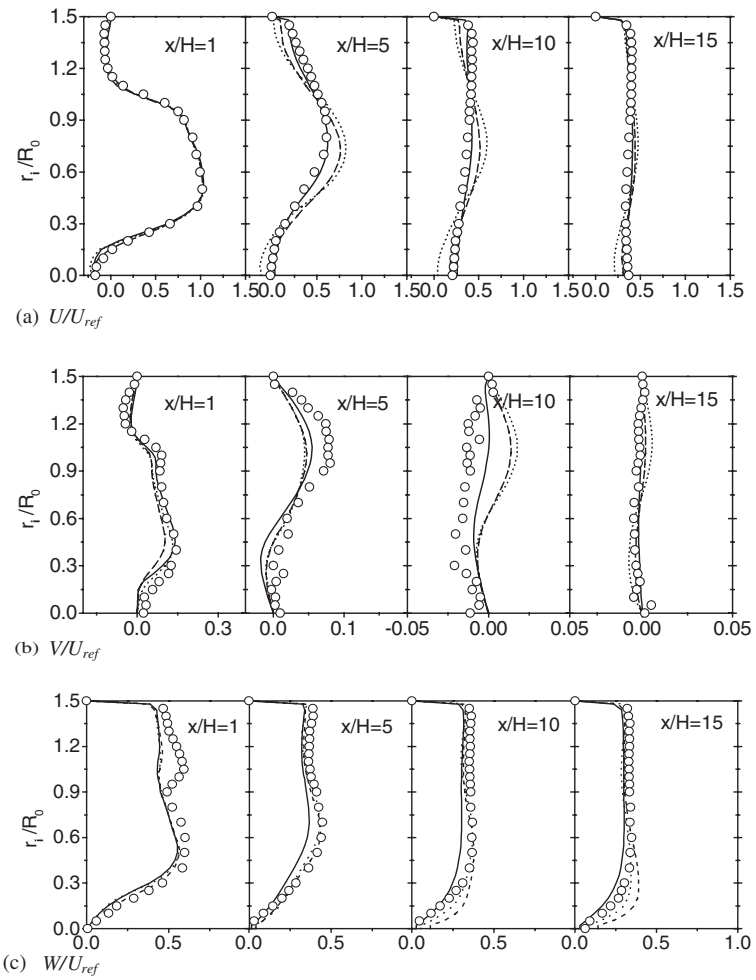

Figure 2. Radial profiles of the non-dimensional mean velocity components.

For the axial velocity component (see Figure 2(a)), U/U_{ref}, it is clear from this figure that, for stations $x/H = 10$ and 15, model 3 exhibits a much better performance than the other two models in predicting the above-mentioned flattening trend, particularly at the near wall region and at the near axis region.

For the radial velocity component (see Figure 2(b)), V/U_{ref}, the reasoning is similar, particularly for the downstream region ($x/H = 10$), where models 1 and 2 even fail to predict the right sign of this velocity component in opposition to the predictions yielded by model 3.

As far as the tangential velocity component (W/U_{ref}) goes (see Figure 2(c)), the comparative performance of the used models is analysed by assessing the predictions and comparing them with the experiments in two distinct flow regions. In the outer flow region ($r_i/R_0 > 1$) the three models predict the experiments with similar accuracy. However, for the inner flow region ($r_i/R_0 < 1$) and for the downstream region ($x/H = 10$ and 15) the velocity profiles predicted by

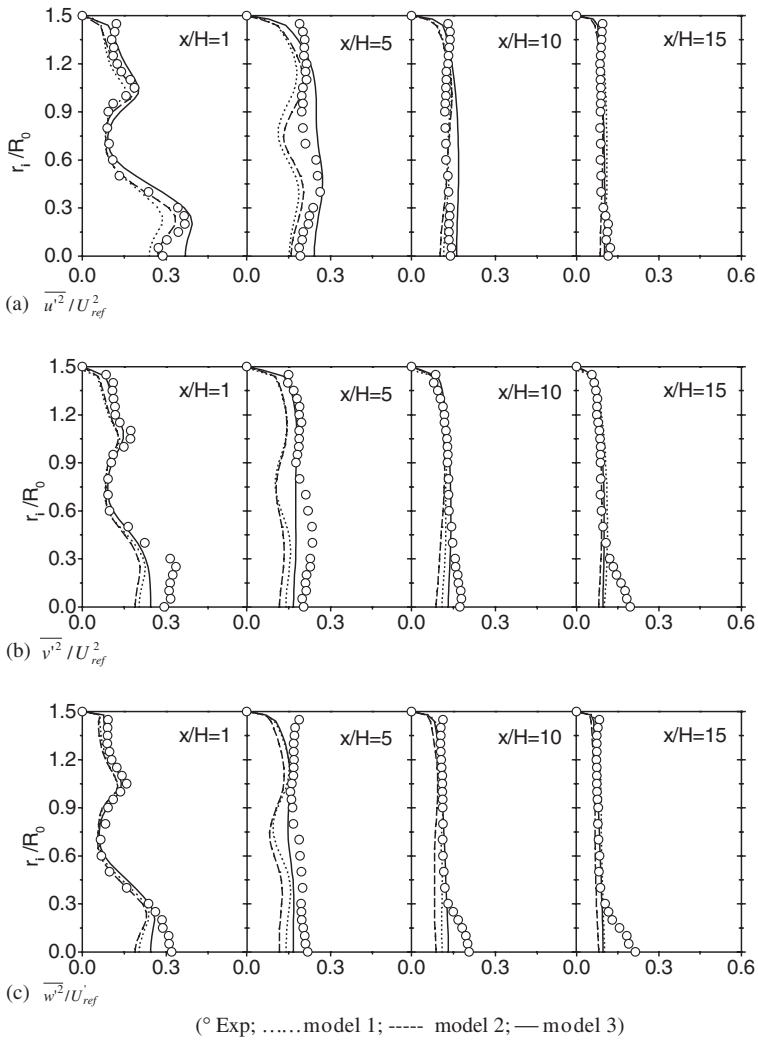

Figure 3. Radial profiles of the non-dimensional normal stresses components.

model 3, although with values slightly underestimated, reproduce the experimental flattening trend with much more evidence than those yielded by models 1 and 2.

Summing up, model 3 predicted the experiments more accurately than the two other models, not only near the wall and near the axis where swirling effects are strong and anisotropy predominates, but particularly in the downstream region of the flow where isotropy may be the predominant feature of turbulence. This means that the proposed equation for the transport of ε—Equation (5) with the modified source term—yields better results than those previously reported in the open literature.

Figure 3 displays the radial profiles of the non-dimensional normal stresses, $\overline{u'^2}/V_{\mathrm{ref}}^2$, $\overline{v'^2}/V_{\mathrm{ref}}^2$ and $\overline{w'^2}/V_{\mathrm{ref}}^2$, at different stations x/H along the axis. All the used models yielded results

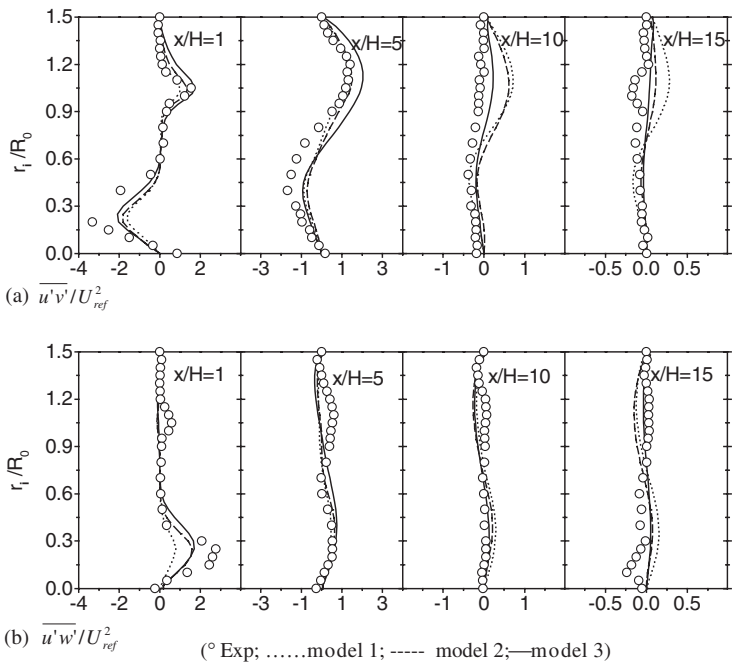

Figure 4. Radial profiles of the non-dimensional mean shear stresses components.

exhibiting, in general, a good agreement with the experimental trends. The differences are mainly referred to the magnitude of the predicted values of the stresses. Model 3, again, performed better than the other two models in predicting all three normal stress components. In the upstream region of the flow ($x/H = 1$), where anisotropy is the predominant feature of turbulence as showed below, model 3 predicted a turbulence intensity higher than the other two models. In the downstream region of the flow, the production of the kinetic energy tends to be very small, due to the flattening effect of the mean velocity profiles. Additionally, in this region, as the dissipation rate of the turbulent kinetic energy is mainly isotropy-controlled, the last term of the source term of the modified equation (5) will dominate and the three models behave similarly.

In the near centreline region and in the region close to wall, all used models yielded predictions with a certain degree of inaccuracy. For $\overline{u'^2}/V_{\mathrm{ref}}^2$ and $\overline{v'^2}/V_{\mathrm{ref}}^2$, the models fail to predict the very rapid decay of the normal stresses in the region close to the wall, although model 3 approaches more closely this trend. For $\overline{v'^2}/V_{\mathrm{ref}}^2$ and $\overline{w'^2}/V_{\mathrm{ref}}^2$, the measurements indicate an increase of the normal stresses in the near centreline region, but none of the models could reproduce this pattern. Other authors (e.g. Reference [28]) have already experienced this flaw of the RSTM.

Figure 4 depicts the radial profiles of the non-dimensional shear stresses, $\overline{u'v'}/V_{\mathrm{ref}}^2$ and $\overline{u'w'}/V_{\mathrm{ref}}^2$, at different axial stations. Model 3 yielded results in better agreement with the experimental trends than the other two models. Indeed, the shear stress values of $\overline{u'v'}/V_{\mathrm{ref}}^2$ in the outer region of the flow were over-predicted at $x/H = 10$ by both model 1 and model 2

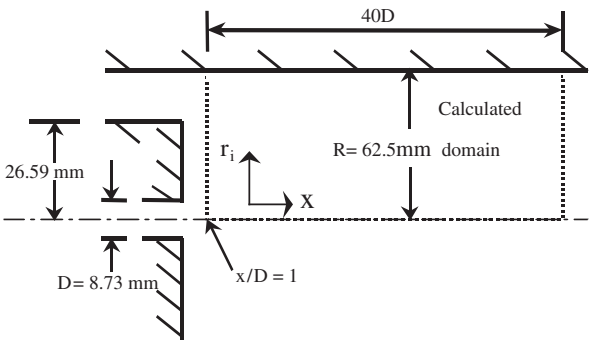

Figure 5. Sketch of the geometry for case 2 (Reference [16]).

and at $x/H=15$ by model 1. For the shear stress $\overline{u'w'}/V_{\text{ref}}^2$, again, model 3 performs better than the other two models at $x/H=15$. At the other axial stations, the three models performed similarly yielding a fairly good agreement between the predictions and the measurements at the inner region of the flow (except model 1 at $x/H=1$), and under-predicted the value of the shear stresses at the outer-region of the flow.

It is also clear from the previous analysis that, at least for this case study, the predictions are much more sensitive to the dissipation rate equation of the turbulent kinetic energy than to the pressure-strain model. In fact, model 2 exhibited a pale improvement when compared with model 1 (effect of the pressure strain modelling), but model 3 yielded much better results than those of model 2 (effect of the ε transport equation). Another point that deserves attention is that model 2 and model 3 performed fairly well in the near wall region, although those models made no recourse to wall-reflection correction terms. This fact encourages the use of the SSG model in complex geometries with turbulent swirling flows.

Case 2: The second geometry studied in this work—case 2—is an annular one and is sketched in Figure 5. The flow inside it is a confined swirling one and experimental data for this flow exist [16]. This case was previously selected by other authors [29–31] to demonstrate the limitations of the k–ε model, in so far as they exist, and the superiority of the RSTM. The flow consists of a central non-swirling jet with a diameter of 8.7 mm and an annular strong swirling jet entering a uniform diameter chamber with an inner radius of $R=62.5$ mm. The rotation motion is induced by a swirler with 15 fixed-vane blades, with a vane angle of 66°, which produces a flow with a swirl number of 2.25.

Predictions with a grid comprising 48×52 nodes, respectively, in the axial and radial directions, are presented. Previous grid independence tests revealed no marked differences. The grid was made particularly denser near the inlet and close to the wall, similarly to case 1.

Experimental data values [16] are referred to the mean axial and swirl velocity components U and W and to the normal stresses $\overline{u'^2}$ and $\overline{w'^2}$ at different axial stations x/D, where D is the diameter of the central jet. As mentioned before the main purpose of the present work is to assess the potential of the new proposed turbulence model, and therefore, boundary conditions at the inlet were specified using the experimental values at $x/D=1$. The radial component of the normal stress, $\overline{v'^2}$, was set equal to the tangential component of that stress, $\overline{w'^2}$. The three

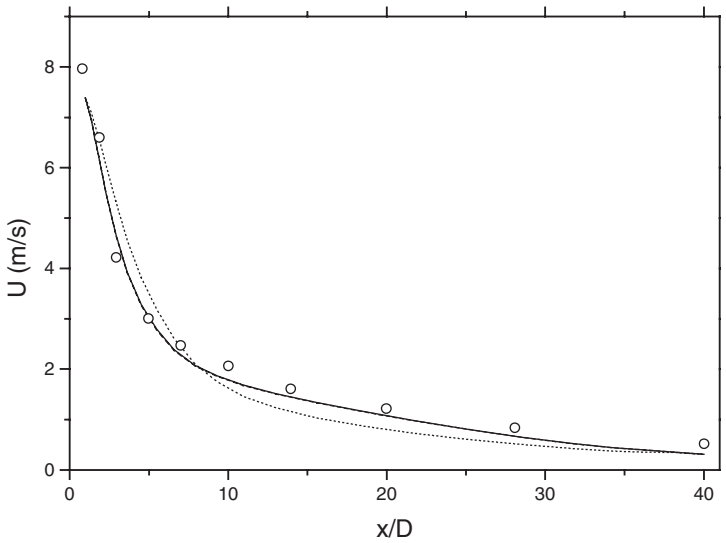

(° Exp; ……model 1; -----model 2; — model 3)

Figure 6. Mean axial velocity component decay along the symmetry axis.

shear stress components, and following the suggestion made in earlier simulations of the same flow [29–31], were assumed to be zero. In order to minimize the sources of possible errors in the predictions, the outlet boundary conditions were prescribed with the available experimental data at the last station, $x/D=40$. In fact, as showed by Reference [29] in their predictions, although the central jet prevents the onset of a reversal flow along the centreline beyond the measurement section that extends up to $x/D=40$, the flow is subcritical there and a developed flow boundary condition at the exit pane is clearly inappropriate.

The same three models used for case 1 were chosen for the simulation of case 2, in order to evaluate and compare the performance of different pressure-strain and turbulent kinetic energy dissipation rate models.

Predicted results and experimental data for the mean velocity components U and W and for the normal shear stress components $\overline{u'^2}$ and $\overline{w'^2}$ are compared in Figures 6–8.

Figure 6 shows the decay of the axial component of the mean velocity at the symmetry axis, for the three tested RSTM models. As it can be seen, the three models could reproduce the main trend of the decay of the referred velocity evidenced by experiments. Moreover, models 2 and 3 yielded almost coincident predictions—the differences are not detectable—and in very good agreement with the experimental values. Comparatively, model 1 yielded predictions not as good as those mentioned above. In fact, results yielded by model 1 exhibit a slower decay of the centreline axial velocity in the region $0<x/D<7$ and a faster decay of the referred velocity at the region $7<x/D<20$. This means that the SSG model appears to be more accurate in the prediction of the centreline axial velocity when compared with the standard LRR model.

The predicted profiles for the axial and tangential velocities at different axial locations are compared with the experiments in Figure 7. Although the agreement is in general fairly good,

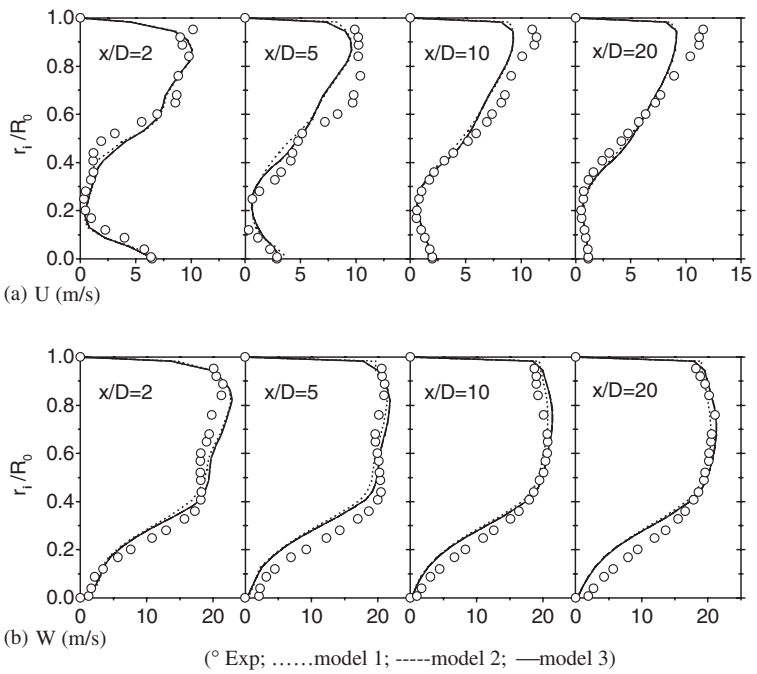

Figure 7. Comparison of radial profiles of U and W velocity components at different axial station against experimental data.

some discrepancies between the predictions and the experiments can be observed. As far as the mean velocity components go, models 2 and 3 yielded almost the same predicted values. This means that for the present case the anisotropic model for the dissipation rate of turbulent kinetic energy has a pale influence in the results.

In more detail, Figure 7 also shows that there are some small differences in the values predicted by model 1 and those predicted by the two other models at the region $0 < r_i/R_0 < 0.6$, particularly for the upstream region. Models 2 and 3 yielded slightly better results than model 1, i.e. SSG model appears to perform slightly better than the standard LRR model for strongly swirling flows.

The predicted axial and tangential components of the turbulent normal stress are plotted in Figure 8 together with the corresponding experimental data. As for the mean velocities, for the normal stresses models 2 and 3 also yielded practically the same predicted values. This confirms the anisotropy is not marked in this strongly swirling flow and, therefore, it has no significant influence in the dissipation rate of the turbulent kinetic energy, as it is explained below. It should be mentioned that model 1 yielded predicted values of the normal stresses much higher than both the experimental values and those obtained with the other two models, particularly for the downstream region of the flow, i.e. $x/D \geq 5$. This strongly suggests that, and simultaneously confirms the conclusion above drawn, for strongly swirling flows the non-linear pressure strain model SSG is more accurate than the LRR model.

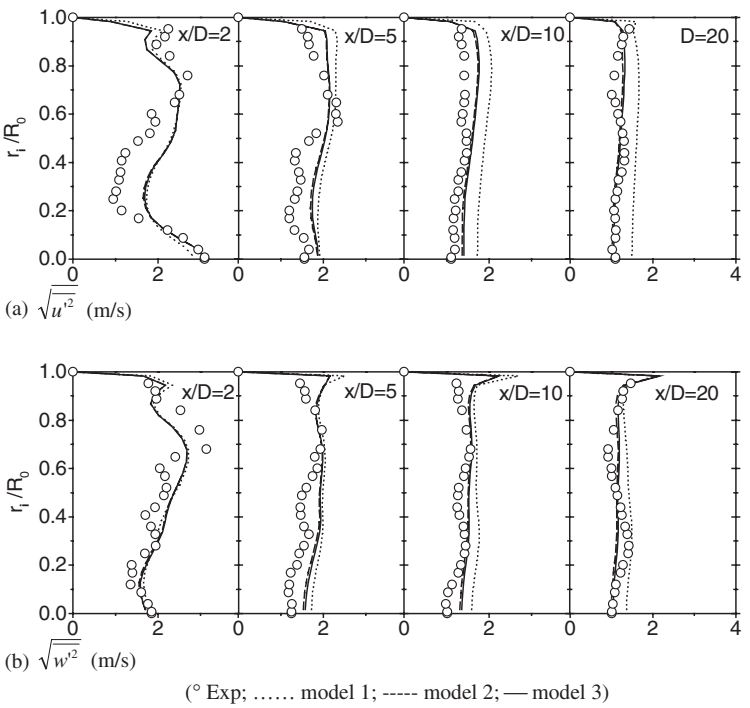

Figure 8. Comparison of radial profiles of normal stresses components at different axial station against experimental data.

In conclusion, from the analysis of the results for case 2 it is clear that for strongly swirling flows, and in opposition to the conclusions drawn for case 1, the predictions are much more sensitive to the pressure-strain model than to the ε transport equation. This means that the SSG model tends to perform better than the standard pressure-strain model, the LRR model, although the latter includes wall-reflection correction terms in its formulation.

Cases comparison: Figure 9 displays the contours of the parameter A—a measure of the anisotropy degree of the flow, as mentioned earlier—for both studied flows. As it can be observed, for case 1 the flow is highly anisotropic in the upstream region of the flow domain ($x/H < 6$) due to swirling effects. In opposition, for case 2, almost all the flow domain is predominantly isotropic—except close to the inlets—as the very high swirl number induces a rapid return to isotropy of this flow. These characteristics of both flows explain the results obtained. In fact, for case 1, for which anisotropy is predominant in the upstream region of the flow domain the new ε transport equation produces a considerable improvement in the accuracy of the results, as anisotropy was considered through the source term of such equation. On the other hand, for case 2, where isotropy is predominant almost all over the flow domain, the pressure-strain correlation term is the one that produces the improvement in the accuracy of the results. This is due to the fact that all the tested turbulence models account for isotropic flow featuring in the source term of the ε transport equation.

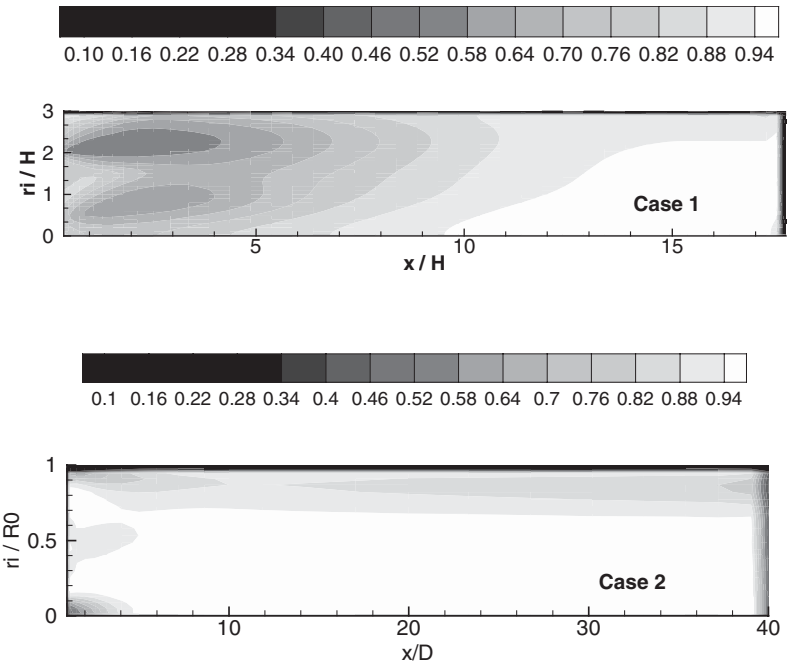

Figure 9. Contours of anisotropy parameter A for the two studied cases.

4. CONCLUDING REMARKS

In the present work, an improved anisotropic dissipation rate model for the turbulent kinetic energy, to be used together with the non-linear pressure-strain SSG model, is proposed. The performance of that new proposed model in predicting confined swirling flows was analysed and compared to that of the standard ε transport equation and different pressure-strain correlation models (LRR and SSG). From the predictions obtained for two isothermal, swirling flows, one weakly swirling (case 1—swirl number of 0.5) and another strongly swirling (case 2—swirl number of 2.25), the following conclusions are drawn.

The SSG model performs very well in the vicinity of walls in both flows, in spite of the fact that it does not contain wall-reflection correction terms in its formulation.

The predictions for case 1 are much more sensitive to the ε transport equation than to the pressure-strain correlation model. The new proposed ε transport equation—with the modified source term running $\varepsilon(2.88A_2P - 1.92\varepsilon)/k$—together with the SSG model, exhibit a strong improvement in accuracy in the predictions for this case study.

All the used models fail to reproduce accurately the experimental trend of the normal stresses to increase their magnitude towards the centreline in case 1.

The predictions for case 2 are much more sensitive to the pressure-strain model than to ε transport equation. The SSG model exhibits a very good behaviour in the predictions of this case study, when compared with the standard pressure-strain model, LRR that comprises wall-reflection correction terms.

NOMENCLATURE

A	Parameter of anisotropy intensity
A_2	Second invariant of anisotropy
A_3	Third invariant of anisotropy
b_{ij}	Reynolds stress anisotropic tensor
C_1	LRR model constant and SSG model constant
C_2	LRR model constant and SSG model constant
C_3	SSG model constant
C_4	SSG model constant
C_5	SSG model constant
C_1^*	SSG model constant
C_3^*	SSG model constant
C_1'	LRR model constant
C_2'	LRR model constant
C_{ij}	Convection term of Reynolds stress transport equation
C_ε	Model constant for the ε transport equation
$C_{\varepsilon 1}$	Model constant for the ε transport equation
$C_{\varepsilon 2}$	Model constant for the ε transport equation
C_s	Diffusion term model constant
C_μ	LRR model constant
D_{ij}	Diffusion term of Reynolds stress transport equation
$f_{x,y}$	Wall correction functions for LRR model
k	Turbulent kinetic energy
$n_{l,i,j,m}$	Unit vectors in the respective directions
p	pressure
p'	pressure fluctuation
P	turbulent kinetic energy production
P_{ij}	production term of Reynolds stress transport equation
S	Swirl number: $S = \int_0^R UWr^2\,\mathrm{d}r / R\int_0^R U^2 r\,\mathrm{d}r$
S_{ij}	mean strain rate tensor
W_{ij}	mean vorticity tensor
$U_{i,j,k}$	mean velocity components in the respective space directions
$u'_{i,j,k}$	velocity fluctuation components in the respective space directions
$\overline{u'_i u'_j}$	Reynolds stresses
$\overline{u'_i u'_j u'_k}$	third order correlation for velocity fluctuations
$x_{i,j,k}$	space directions
x_n	axial distance to the wall
y_n	radial distance to the wall

Greek characters

δ_{ij}	Kronecker operator
ε	rate of dissipation of k
ε_{ij}	dissipation term of Reynolds stress transport equation
Φ_{ij}	pressure strain term of Reynolds stress transport equation

$\Phi_{ij,1}$ return to isotropy term in the pressure strain model
$\Phi_{ij,2}$ rapid term in the pressure strain model
$\Phi_{ij,w}$ wall correction terms
$\Phi^{1,2}_{ij,w}$ wall correction terms to $\Phi_{ij,1}$ and $\Phi_{ij,2}$
κ Von Karman constant
μ viscosity
ρ density

ACKNOWLEDGEMENTS

This work has been partially performed with the financial support of the European Collaborative Research JOULE Programme, under the contract JOE3-CT97-0070. The authors are also grateful to the financial support from Fundacão para a Ciência e Tecnologia of Portugal through the Ph.D. scholarship (PRAXIS XXI/BD/16094/98) granted to Lu Pisi.

REFERENCES

1. Launder BE, Spalding DB. The numerical computation of turbulent flows. *Computer Methods in Applied Mechanics and Engineering* 1974; **3**:269–289.
2. Carvalho MG, Oliveira P, Semião V. A three-dimensional modelling of an industrial glass furnace. *Journal of the Institution of Energy* 1988; **LXI**(448):143–156.
3. Carvalho MG, Semião V, Coelho P. Modelling and optimization of the NO formation in an industrial glass furnace. *ASME Journal of Engineering for Industry* 1992; **114**:514–523.
4. Yuan J, Semião V, Carvalho MG. Predictions of particulate formation, oxidation and distribution inside a three-dimensional oil-fired furnace. *Journal of the Institution of Energy* 1997; **LXX**(483):57–70.
5. Launder BE, Morse AP. Numerical prediction of axisymmetric free shear flows with a Reynolds stress turbulence closure. In *Turbulent Shear Flows*, vol. 1, Durst F *et al.* (eds). Springer: Berlin, 1979; 279–294.
6. Lockwood FC, Shen B. Performance Predictions of Pulverised-coal flames of power station furnace and cement kiln types. *Twenty-fifth Symposium* (*International*) *Combustion*, The Combustion Institute, 1994; 503–509.
7. Lu P, Ye T, Costa M, Semião V, Carvalho MG. Prediction with a second moment closure turbulence model and experiments of combined combustion of pulverized coal and propane in a semi-industrial combustor. *Proceedings of the 4th International Symposium on Coal Combustion*, Beijing, China, 1999; 356–367.
8. Launder BE. Second-moment closure: Present ... and future? *International Journal of Heat and Fluid Flow* 1989; **10**:292–300.
9. Hanjalic K. Advanced turbulence closure models: a view of current status and future prospects. *International Journal of Heat and Fluid Flow* 1994; **15**:178–203.
10. Hanjalic K. Second-moment turbulence closure for CFD: need and prospects. *International Journal of Computational Fluid Dynamics* 1999; **12**:67–97.
11. Lumley JL, Khajeh-Nouri BJ. Computational modelling of turbulent transport. *Advances in Geophysics* 1974; **18A**:169–192.
12. Speziale CG, Sarkar S, Gatski TB. Modelling the pressure-strain correlation of turbulence: an invariant dynamical systems approach. *Journal of Fluid Mechanics* 1991; **227**:245–272.
13. Basara B, Younis BA. Assessment of the SSG pressure-strain model in two-dimensional turbulent separated flows. *Applied Scientific Research* 1995; **55**:39–61.
14. Younis BA, Gatski TB, Speziale CG. Assessment of the SSG pressure-strain model in free turbulent jets with and without swirl. *ASME Journal of Fluids Engineering* 1996; **118**:800–809.
15. Ahmed SA, Nejad AS. Velocity measurements in a research combustor—Part 1: Isothermal swirling flow. *Experimental Thermal and Fluids Science* 1992; **5**:162–174.
16. So RM, Ahmed SA, Mongia HC. An experimental investigation of gas jets in confined swirling airflow. *NASA CR 3832*, 1984.
17. Launder BE, Reece GJ, Rodi W. Progress in the development of a Reynolds-stress turbulence closure—Part 3. *Journal of Fluid Mechanics* 1975; **68**:537–566.
18. Daly BJ, Harlow IH. Transport equations in turbulence. *Physics of Fluids* 1970; **13**:2634–2649.
19. Rotta JC. Statistische theorie nichthomogener Turbulenz. *Izvertiya Physik* 1951; **129**:547–573.
20. Naot D, Shavit A, Wolfstein M. Interaction between components of the turbulent velocity correlation tensor. *Israel Journal of Technology* 1970; **8**:259–269.

21. Shir CC. A preliminary numerical study of atmospheric turbulent flows in the idealised planetary boundary layer. *Journal of the Atmospheric Sciences* 1973; **30**:1327–1339.
22. Gibson MM, Launder BE. Ground effects on pressure fluctuations in the atmospheric boundary layers. *Journal of Fluid Mechanics* 1978; **86**:491–551.
23. Gibson MM, Younis BA. Calculation of swirling jet with a Reynolds stress closure. *Physics of Fluids* 1986; **29**:38–48.
24. Pope SB. An explanation of the turbulent round-jet anomaly. *AIAA Journal* 1978; **16**:279–281.
25. Hanjalic K, Launder BE. Sensitizing the dissipation equation to irrotational strains. *ASME Journal of Fluids Engineering* 1980; **102**:34–40.
26. Aupoix B, Cousteix J, Liandrat J. Effect of rotation of isotropic turbulence. *Proceedings of the 4th Symposium on Turbulent Shear Flows*, Karlsruhe, Germany, 1983; 9.7–9.12.
27. Tavoularis S, Corrsin S. Experiments in nearly homogeneous turbulent shear flow with a non uniform mean temperature gradient—Part I. *Journal of Fluid Mechanics* 1981; **104**:311–347.
28. Hogg SI. Second-moment-closure calculations of strongly-swirling confined flows with and without density variations. *Ph.D. Thesis*, Mechanical Engineering Department, UMIST, Manchester, UK, 1988.
29. Hogg SI, Leschziner MA. Computation of highly swirling confined flow with a Reynolds stress turbulence model. *AIAA Journal* 1989; **27**:57–63.
30. Jones WP, Pascau BA. Calculation of confined swirling flows with a second moment closure. *ASME Journal of Fluids Engineering* 1989; **111**:248–255.
31. Sharif MAR, Wong YKE. Evaluation of the performance of three turbulence closure models in the prediction of confined swirling flows. *Computational Fluids* 1995; **24**(1):81–100.

